Astron. Astrophys. 329, 809–820 (1998)

ASTRONOMY AND ASTROPHYSICS

Large rotation measures in radio galaxies at z > 2

R.M. Athreya[1], **V.K. Kapahi**[1], **P.J. McCarthy**[2], **and W. van Breugel**[3]

[1] National Centre for Radio Astrophysics (TIFR) P.O.Bag 3, Pune University Campus, Pune 411 007, India (ramana@gmrt.ernet.in (RMA) and vijay@gmrt.ernet.in (VKK))
[2] Observatories of the Carnegie Institution of Washington, 818, Santa Barbara St., Pasadena, CA 91107, USA
[3] IGPP, Lawrence Livermore National Laboratories, P.O.Box 808, Livermore, CA 94550, USA

Received 20 November 1996 / Accepted 26 June 1997

Abstract. We have carried out multifrequency radio polarisation imaging of a sample of 15 radio galaxies at z > 2 from the MRC/1Jy sample using the VLA. We report here the discovery of large rotation measures (RM) in a considerable fraction of the high redshift radio galaxies. Using the difference between the RM values of the two radio lobes in each source and statistical arguments, we show that the Faraday screens responsible for the RMs are most likely to be in the vicinity of the radio sources themselves. Four of the 15 galaxies show intrinsic (redshift corrected) RMs in excess of 1000 rad m^{-2} with the highest value of ∼6000 rad m^{-2} in 1138-262 at z = 2.17. These observations suggest that the environments of the radio galaxies at z > 2 have micro gauss magnetic fields correlated over many kpc (>5–10), at least.

We have discussed the problems due to the short time available at those redshifts for the various mechanisms, which are believed to generate and correlate strong magnetic fields on large scales, to operate. In particular, we argue that, unlike at low redshifts, cluster cooling flows are unlikely to have a role in forming deep Faraday screens at high redshifts. It is not clear if the dynamo mechanism is capable of generating such fields in the ambient medium around the radio sources. It appears plausible that condensates of magnetised plasma (galactic or subgalactic sized) are the deep Faraday screens responsible for the observed RMs. We suggest that plasma clumps of as small as 10^9 $M_\odot$ in the path of the radio jet may generate very large RMs.

The presence of such strong and large scale magnetic fields in the medium around the radio sources at such early epochs poses a considerable challenge to models of the origin of magnetic fields in the Universe.

Key words: galaxies: magnetic fields – radio continuum: galaxies – cosmology: observations

Send offprint requests to: R.M. Athreya

1. Introduction

We have undertaken a detailed radio study of a sample of 15 radio galaxies at z > 2 (Athreya 1996; Athreya et al. 1997a, b) from the newly defined MRC/1Jy complete sample of extragalactic radio sources (McCarthy et al. 1996; Kapahi et al. 1997a, b). One of the primary aims of defining and studying the MRC/1Jy sample was to discover a large and unbiased sample of high redshift radio galaxies (HRRG) for further study. In addition to their many interesting properties, the radio sources in these galaxies are useful as probes of the environment at high redshifts; it is hoped that studies of these objects will considerably improve our understanding of the earliest epochs of galaxy formation.

Our radio observations of the 15 galaxies provide the first extensive data-set to study the general properties of the radio galaxy population at z > 2.0. The discovery of steep spectrum radio cores in a majority of these galaxies has been discussed in detail by Athreya et al. (1997a). Results from this study on other aspects including morphology, energetics, spectra, etc. will be discussed in subsequent papers.

We discuss in this paper the large RMs observed in the sample of radio galaxies at z > 2, including an intrinsic (redshift corrected) RM of ∼6000 rad m^{-2} in the galaxy 1138-262 at z = 2.17. We also discuss the various mechanisms which have been suggested for generating and aligning magnetic fields and examine these in the light of the much smaller age of the Universe at those redshifts and hence the shorter time available for these processes to operate.

The Rotation measure (RM), which is the slope of the straight line fit to the Polarisation position angle (PPA) *versus* λ^2 (λ : wavelength), may be related to the thermal (as against relativistic) electron density n_e, magnetic field B and the size L of the screen responsible for the Faraday rotation by

$$RM = \int_o^L n_e(s)\ \boldsymbol{B}(s) \cdot d\boldsymbol{s}, \qquad (1)$$

where, the line element ds is along the path of the radiation. A more *practical* relationship to estimate average values of the

physical parameters (equivalent to assuming uniform electron density and magnetic field; in case of field reversal(s) within the screen, the values obtained from this relationship would be lower limits to the actual values) is

$$RM \;=\; 810\, n_e\, B_{\parallel}\, L, \qquad (2)$$

where RM is in radian m^{-2}, n_e in cm^{-3}, L in kpc and $\mathrm{B}_{\parallel}$, the parallel component of the magnetic field in micro gauss (μG). The RM is an algebraically additive quantity and all intervening Faraday screens contribute to the RM of a background source. The observed RM is given by $RM_{obs} = \sum_F [RM_i^F/(1 + z_F)^2]$, where RM_i^F is the intrinsic RM of the screen at redshift z_F and the sum is over all Faraday screens (F) along the line of sight to the radio source. Studies of astrophysical magnetic fields are often based on RM observations though RM provides only an indirect estimate of the magnetic field since it requires independent estimates of the electron density, path length and the redshift(s) of the Faraday screen(s) which are not always available.

RMs of low redshift radio galaxies: Most radio galaxies at low redshift show observed RM of $<30\,\mathrm{rad\,m^{-2}}$ (Tabara & Inoue 1980; Leahy et al. 1980). Much of this RM is believed to arise in the interstellar medium (ISM) of our Galaxy (Simard-Normandin et al. 1981; Leahy 1987). However not all the RM is due to the ISM in our galaxy and, in particular, a small fraction of radio galaxies have very large RMs originating close to the source. Of the hundreds of low redshift radio galaxies (z < 1) studied, about 15–20 sources have RM $> 700\,\mathrm{rad\,m^{-2}}$ (e.g. Taylor et al. 1992, 1994). The largest RM known is $\sim$20,000 $\mathrm{rad\,m^{-2}}$ in 3C 295 (Perley & Taylor 1991). Such radio sources are either compact (sub-galactic) in size or are found in x-ray clusters with cooling flows. An excess of RM has been observed in sources located behind the centres of dense clusters indicating that the clusters are responsible for it (Kim et al. 1991). The association of large RM sources with cooling-flow clusters (Taylor et al. 1994) has led to the belief that cooling-flows are in some way responsible for setting up the deep Faraday screens.

RMs of radio galaxies at z ∼ 1: The polarisation properties of a sample of 7 sources from the 3CR at 0.6 < z < 1.2 and Galactic latitude $|b| > 20^\circ$ were studied by Pedelty et al. (1989). The median RM_{obs} for the sample, considering only the highest value in each radio lobe, was $19\,\mathrm{rad\,m^{-2}}$, the highest value for the sample being $86\,\mathrm{rad\,m^{-2}}$. A more pertinent quantity for comparison with the present study is the mean RM_{obs} value for each lobe (i.e. the average of the different RM values measured within the resolved radio lobe); the sample has a median of $12\,\mathrm{rad\,m^{-2}}$ with the highest being $60\,\mathrm{rad\,m^{-2}}$. The median RM_i for the sample, assuming a Faraday screen close to the radio source, is $40\,\mathrm{rad\,m^{-2}}$ while the highest value is $197\,\mathrm{rad\,m^{-2}}$.

RMs in intervening galaxies: Several studies have dealt with the RMs of distant core-dominated quasars (Welter et al. 1984; Oren & Wolfe 1995). The absorption-line systems seen in the optical spectra of distant quasars may introduce a Faraday rotation in the background radio quasar. Unfortunately, the compact quasars sample only one line of sight through the intervening systems and it is very difficult to separate the RM contributions from our Galactic ISM, the absorption-line systems, the circum-quasar material and the RM intrinsic to the quasar core.

Table 1. Polarimetric observations of MRC/1Jy high redshift radio galaxies (z > 2) using the VLA. The mean frequencies are given within angular brackets. The project codes are VLA AA155 (code A) and VLA AC374 (code C). The bandwidth is 50 MHz at all frequencies.

frequencies GHz	Array	Resoln. arcsec	Proj. code	Date
1.465,1.385 ⟨1.43⟩	BnA	3.0–4.0	A	14 Feb 93
4.535,4.885 ⟨4.71⟩	A	0.4–0.9	C	18 Mar 94
4.835,4.885 ⟨4.86⟩	BnC	3.0–4.0	A	24,30 May 94
8.085,8.335 ⟨8.21⟩	A	0.2–0.4	C	18 Mar 94
8.415,8.465 ⟨8.44⟩	BnA	0.5–0.7	A	14 Feb 93

2. Observations and analyses

2.1. Sample selection

Radio, optical and infrared observations of the 558 sources in the MRC/1Jy sample have resulted in the discovery of about 40 sources at z > 2 (McCarthy et al. 1997). The redshifts of 19 of these have been confirmed spectroscopically while the rest have been estimated from the well known relationship between infrared K-band magnitude and redshift (Lilly 1989; McCarthy 1993). The optical identification of the sample is complete to 95 per cent (McCarthy et al. 1996) while redshift information (spectroscopic or from K-magnitudes) is available for 80 percent of the galaxies. We do not think that the incompleteness of the spectroscopy has biased the HRRG sample seriously since the incompleteness is essentially due to paucity of observing time at some right ascensions. There were 17 galaxies known in 1993 with spectroscopic z > 2. High resolution multifrequency observations of 15 of them were undertaken in 1993 using the VLA radio telescope. The other two sources could not be observed due to constraints imposed by the range of LST allocated to our project. These 15 radio galaxies are unlikely to be significantly biased in any respect and are expected to be representative of the z > 2 galaxies in the MRC/1Jy sample.

2.2. Observations

The details of the observations of the 15 HRRGs are listed in Table 1. The sources were observed for 10–30 minutes in 3–5 bands, each band consisting of 2 frequencies of 50 MHz bandwidth. The observations for each source were split into several (2–4) shorter sessions at different hour angles to improve the u-v coverage. The flux calibration was done from observations of 3C 48 and 3C 286 on the scale of Baars et al. (1977) together

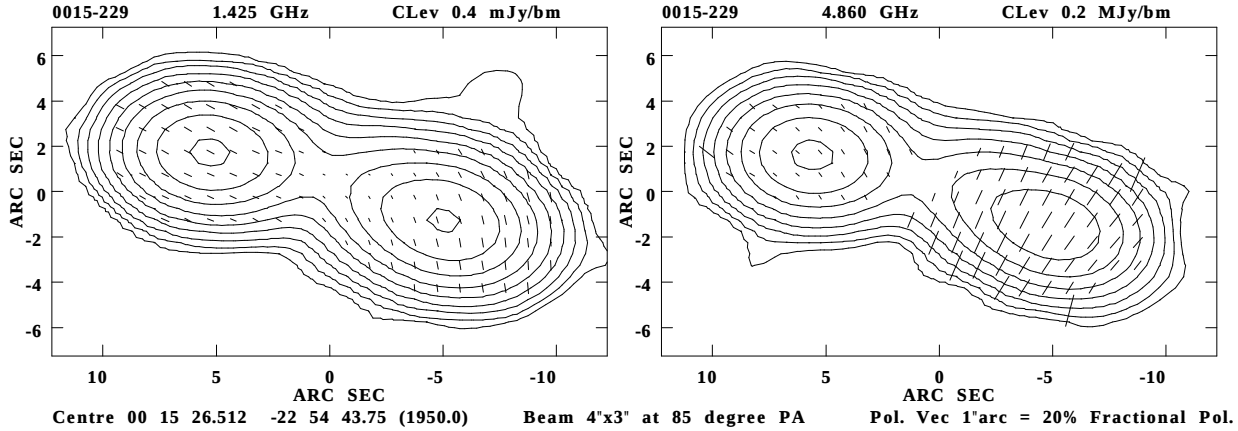

Fig. 1. Radio contour images of 0015-229 (z = 2.01) with polarisation vectors superposed. The co-ordinates of the centre, the beam size and the scale for polarised flux, which are common for both the images, are listed below them. The frequency and the contour scale factor (CLev) are listed above the images. The contour levels are Clev × [-2, -1, 1, 2, 4, 8, 16, . . .]. The superposed vectors indicate the direction and magnitude of the fractional polarisation.

with the recent corrections determined by Perley in AIPS[1] (see the HELP files on AIPS version 15JULY95). The phase calibration and determination of the instrumental polarisation was done using 0237-233, 1143-245 and 2331-240. The PPA was calibrated using 3C 138 (-9° at 1.425 GHz and -12° at higher frequencies) and 3C 286 (33° at all frequencies).

2.3. Data reduction

The data were analysed in a standard manner using the AIPS package. After the initial flux density, phase and polarisation calibration, the visibility data were passed through 3–4 rounds of SELF-CAL (phase only) to obtain an rms noise of ∼0.05–0.15 mJy/bm in the final images.

For each source, the best quality Stokes I image was obtained by the procedure described above. The same data was used to obtain images in Stokes Q, U and V. This was done independently at both frequencies in each band. Since extended extragalactic sources are not expected to have any circular polarisation, the V images, expected to be pure noise images, were used to estimate the quality of the calibration procedure. At 8.4 GHz, in addition to the high resolution images, lower resolution images similar to those at 1.4 and 4.8 GHz were made by weighting down the long baselines during analysis. This was necessary since polarisation properties are known to be resolution dependent. Similarly, matched higher resolution images were also obtained at 4.71, 8.21 and 8.44 GHz.

UV-tapering of the 4.71 and 8.21 GHz data to obtain lower resolution images similar to those at 1.43 and 4.86 GHz did not prove successful. The short duration of the 4.71 and 8.21 GHz observations in the A array configuration resulted in very few short baselines and the weighting down of the much more numerous long baselines reduced drastically the effective number of baselines leading to excessively noisy images.

The Stokes images were used to obtain maps of total polarisation (P = $\sqrt{Q^2 + U^2}$) and the PPA ($\Psi = \tan^{-1}(U/Q)$) by combining the images appropriately, pixel by pixel. The total polarisation images were corrected for the Ricean bias in the noise statistics.

2.4. Rotation measure calculation

The resolutions at 1.43 and 4.86 GHz (3–4″) are similar to the sizes of the individual radio lobes and hence inadequate for studying the variation of polarisation properties across the lobes. So the PPA data presented here as well as the RM calculated from them are (polarized flux weighted) average values for the entire lobe. The higher resolution images at 4.71 and 8.21 were from shorter duration observations at fewer hour angles and it was found that the measurements were not very reliable at faint polarised flux levels. So the PPA measurements in these images were also confined to the area around the hotspots, which had high signal-to-noise ratio.

The PPA was obtained by averaging the values within a box (9–25 pixels) centred around the peak of the polarised emission for each radio lobe. The shift in the peak positions between different frequencies was found to be <1 pixel (beam width 5–8 pixels along each axis). The radio contour maps of 0015-229, which are typical of the sample, are shown in Fig. 1. The radio polarisation maps of all the sources are being published elsewhere (Athreya et al. 1997b) together with all the other images and data.

A 5σ detection threshold was considered sufficient for the polarised flux. RMs were calculated only for those radio lobes which were detected in at least 2 different bands (i.e. 3–4 frequencies). Most of the detections were at the level of ∼10σ and the errors on the PPA values are 5–10° (including the 2–3° error in the primary PPA calibrator).

[1] Astronomical Image Processing System, distributed by the National Radio Astronomy Observatories, USA.

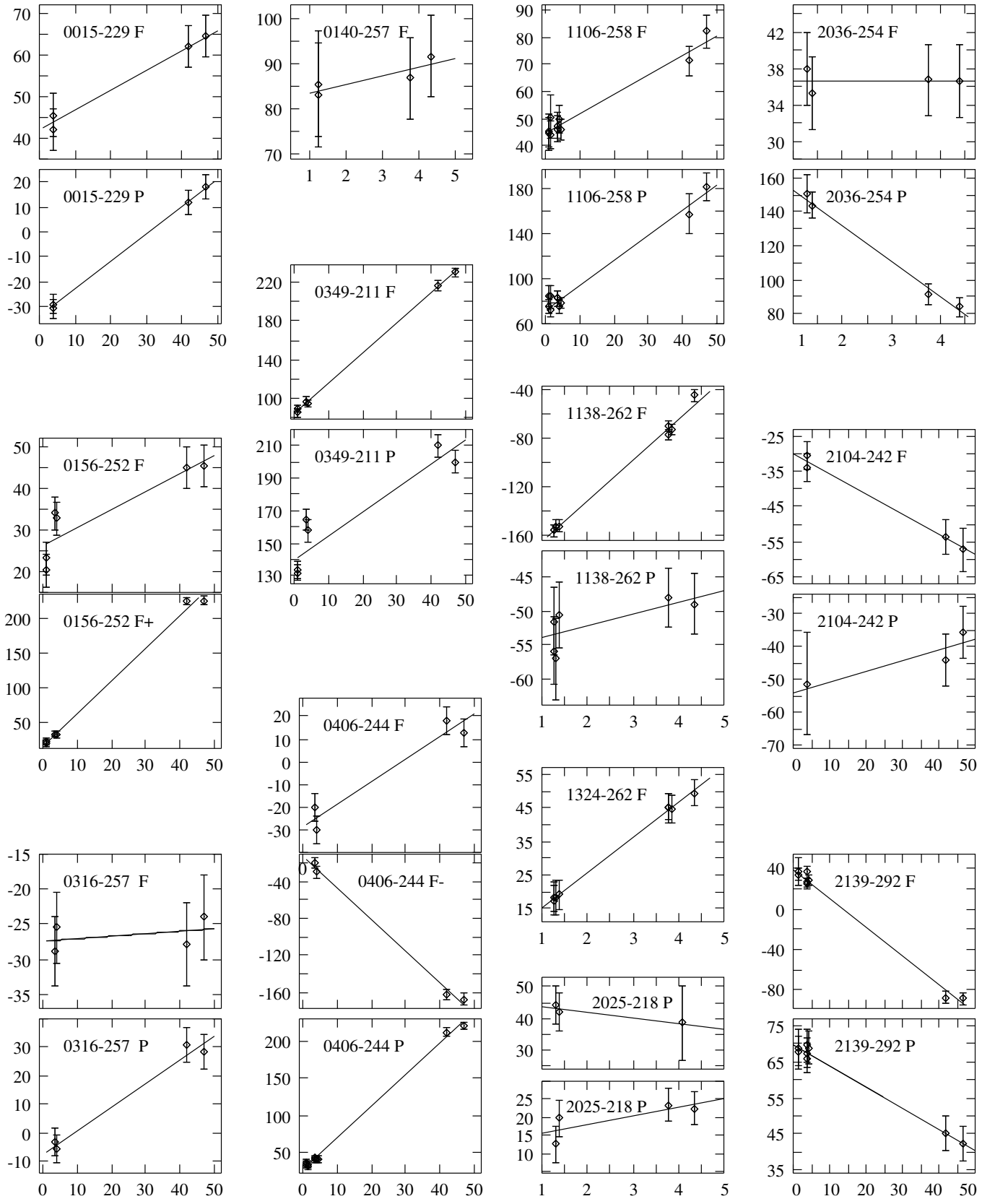

Fig. 2. Polarisation position angle in degrees (y-axis) *v/s* λ^2 in $10^{-3}\,\mathrm{m}^{-2}$ (x-axis) for the lobes of MRC/1Jy galaxies at z > 2. The F or P following the source names indicate the Following and Preceding lobes, respectively. Two plots are shown for each of 0156-252 F and 0406-244 F, with an additional 180° rotation.

Table 2. Observed rotation measures in the lobes of MRC/1Jy galaxies at z > 2. The columns are redshift (z), remarks (R), observed RM (RM_{obs}), flux density at 4.86 GHz ($S_{4.86}$) and the fractional polarisation (%-pol) within parantheses, residuals of the linear fit (δ: $\langle\rangle$ the mean of the residuals and Mx the maximum value), reduced χ^2 and number of points (N) of the fit. The remarks are 'a' (an additional 180° rotation given to the PPA of 1.425 GHz), 'l' (low resolution images: 3–4 arcseca) and 'h' (high resolution images (0.5–0.7 arcsec).

source	R	Following lobe				Preceding lobe			
		RM_{obs} rad m^{-2}	$S_{4.86}$ (%-pol) mJy	δ° $\langle\rangle$ Mx	χ^2 (N)	RM_{obs} rad m^{-2}	$S_{4.86}$ (%-pol) mJy	δ° $\langle\rangle$ Mx	χ^2 (N)
0015-229	l	8.3 ± 2.1	33 (4.5 ± 0.5)	0.9 1.7	0.12 (4)	19.3 ± 1.9	29 (14.6 ± 1.5)	0.7 1.0	0.07 (4)
0140-257	h	Polarised flux in 1 band only				33.4 ± 63	39 (5.1 ± 0.5)	1.6 2.1	0.06 (4)
0156-252	l	7.5 ± 1.7	87 (6.6 ± 0.7)	3.8 6.6	1.84 (6)	No polarised flux detected			
	a,l	82.0 ± 1.7		4.6 12.1	2.71 (6)				
	h	160 ± 31			(4)	No polarised flux detected			
0316-257	l	0.6 ± 2.4	37 (2.3 ± 0.2)	1.8 2.0	0.23 (4)	14.5 ± 2.4	61 (2.1 ± 0.2)	2.3 3.5	0.38 (4)
0349-211	l	54.8 ± 1.7	61 (8.2 ± 0.8)	1.4 2.3	0.20 (6)	25.9 ± 2.2	50 (1.5 ± 0.2)	11.1 19.7	5.50 (6)
0406-244	l,h	17.3 ± 2.6	31 (2.2 ± 0.4)	5.0 5.4	1.41 (4)	74.4 ± 1.6	70 (7.5 ± 0.8)	3.6 6.9	0.66 (10)
	a,l,h	-59.6 ± 2.6		5.3 6.2	1.61 (4)				
1106-258	l,h	12.7 ± 1.9	12 (16.1 ± 2.4)	2.0 5.3	0.12 (10)	38.7 ± 4.3	31 (4.0 ± 0.8)	4.8 9.6	0.53 (10)
1138-262	l,h	588 ± 22	50 (3.8 ± 0.4)	2.6 6.2	0.72 (8)	31.1 ± 26	106 (3.5 ± 0.3)	2.1 3.6	0.27 (6)
1324-262	l,h	183 ± 20	63 (7.5 ± 1.1)	0.5 1.1	0.03 (8)	No polarised flux detected			
2025-218	h	-30.4 ± 77	36 (1.5 ± 0.5)	0.6 0.8	0.04 (3)	42.5 ± 30	55 (10.8 ± 0.6)	2.3 3.6	0.56 (4)
2036-254	h	0.3 ± 25	50 (16.1 ± 1.6)	0.7 1.4	0.12 (4)	-369 ± 48	37 (2.7 ± 0.5)	2.5 4.0	0.25 (4)
2104-242	l	-10.0 ± 2.1	54 (7.1 ± 0.7)	1.1 1.6	0.17 (4)	5.7 ± 7.0	6.5 (6.1 ± 2.0)	6.0 7.8	0.35 (3)
2139-292	l,h	-49.8 ± 2.0	43 (5.3 ± 0.5)	3.9 7.7	0.89 (8)	10.3 ± 1.7	72 (18.7 ± 1.9)	0.9 2.0	0.10 (8)

Notes: i. RMs calculated using a combination of low and high resolution images are indicated by l,h under remarks .
ii. Only the highest RM has been listed here in the case of multiple components in a radio lobe.
iii. The multiple RM fits in 0156-252 and 0406-244 are explained in the text.
iv. The flux density errors are ∼5 per cent.

Lack of resolution at lower frequencies forced us to observe at frequencies > 1.4 GHz. The rather small difference in the rest frame λ^2 among the 3 bands (particularly between 4.71 and 8.4 GHz) resulted in considerable errors on the intrinsic RM values despite the large number of frequencies of observation.

The (n×180°) ambiguity of the PPA was resolved in most cases by examining the PPA change between closely spaced frequencies (actually closely spaced in λ^2) – 1.3851 & 1.4649 GHz, 4.5351 & 4.8851 GHz, 4.86 & 8.44 GHz bands. The 180° ambiguity in the PPA implied that we were incapable of measuring observed RMs in excess of ∼1200 rad m^{-2} (or ∼630 rad m^{-2} in objects without the 4.71 GHz band observations), which corresponds to intrinsic RMs at z > 2 of $\gtrsim$12000 rad m^{-2} (or ∼6300 rad m^{-2}). A straight line was then fit to all the data points to obtain a RM consistent with the value obtained from the close pairs. The smallest value of the RM was found to provide the best fit to the data of all radio lobes excepting two (explained in the notes on individual sources). The change in PPA with frequency can also be caused by many independent polarised components within the telescope resolution. Multiple components with very different spectral indices and fractional polarisation may mimic Faraday rotation with the PPA of different components dominating at different frequencies. However, a linear relationship between the PPA and λ^2 is the signature of Faraday rotation.

The PPA from low and high resolution observations were combined to calculate the RM in several sources (indicated in Table 2). However, it was first checked that the measured PPA values from images of different resolutions but at similar frequencies were consistent with each other (∼4.8 GHz images from the A and CnB configurations, untapered and tapered 8.44 GHz images from the BnA config. and untapered 8.21 GHz images from A config.).

This may be verified in Fig. 2 from the plots for 0406-244 P, 1106-258, 1138-262, 1324-262, 2139-292 (these being the only sources with a mixture of PPA from different resolutions). In each case, each of the clusters of points at $\lambda^2 \approx 1.3$ and 3.8, consists of 3–4 data points obtained from images at 2 different resolutions. The consistency between the values from different resolutions suggests that either the polarised flux is dominated by the emission from the immediate vicinity of the hotspot (2–5 kpc) or the same Faraday screen covers all parts of the radio lobe contributing substantially to the observed polarised flux.

3. Results

The PPA–λ^2 plots are shown in Fig. 2. The RMs and the statistics of the fit are listed in Table 2.

As mentioned earlier, RM studies, particularly involving low resolution observations in which the magnetic field structure is unresolved, have to consider the crucial question of whether or not the observed change of PPA with frequency is due to Faraday Rotation (or merely due to unresolved multiple components). In view of this, Table 2 also lists some parameters which quantify the quality of the straight line fit to the points in the PPA– λ^2 plane. The parameters listed include the mean of the absolute

value of the deviation from the fit, the largest deviation and the reduced χ^2 along with the number of points in the fit.

The errors on the PPA values used here have been calculated by adding in quadrature the errors due to polarisation calibration (5° for 1.425 GHz bands and 3° for 4.8 and 8.4 GHz, the difference being due to the larger effect of the ionosphere at lower frequencies) and due to those on Stokes Q and U flux density.

The reduced χ^2 is <1 in 20 of the 23 lobes (and much less in many) indicating that the straight line is indeed a good fit in most cases. The sources for which the χ^2 values are large are 0156-252 foll. lobe (low resolution image), 0406-244 foll. lobe and 0349-211 prec. lobe. However, it must be noted that the χ^2 is critically dependent on the formal error assigned to each point and in fact one very discrepant point could affect the statistic to a large extent. In fact, an examination of the residuals shows that the mean and the maximum residuals are only 3.8° and 6.6° in 0156-252 and 5.0° and 5.4° in 0406-244. This indicates that either the error has been underestimated by a few (1–3) degrees in the case of a few points or that those points have been contaminated at the same level (i.e. 1–3°) by PPA changes due to multiple components. The low value of the χ^2 and/or the small mean deviations of a few degrees seen in almost all sources justifies our assigning Faraday rotation as the cause for the change of PPA with frequency. However, the residuals and the χ^2 value seen in the case of 0349-211 prec. lobe are too large to be assigned to random error in the PPA values and multiple components could be the explanation.

Some notes on the RM calculations of individual sources are given below :
0030-219: An unresolved source with no polarised flux detected.
0140-257: *foll. lobe* - No polarised flux detected.
0156-252: *foll. lobe* - RM values of both 7.5 and 82 rad m^{-2} fit the data from low resolution images. At higher resolution, the lobe is well resolved and consists of the hotspot, parts of the jet and extended emission surrounding the two. The higher resolution image (see Fig. 3) shows a large variation in the RM$_{obs}$ ranging from 18 to 160 rad m^{-2} . This source clearly shows the effect of low resolution on RM. The areas with low RM contribute most of the polarised flux and so the integrated RM from low resolution images is much smaller.
prec. lobe - No polarised flux detected.
0406-244: *foll. lobe* - It is difficult to resolve the 180° ambiguity and two values of the RM make for equally good fits.
prec. lobe - An increase of 180° in the PPA at 1.425 GHz resulted in an excellent fit. There is a good agreement between the PPA values in the high and low resolution images. There are 4 data points (several of them superposed in the plots) in both the 4.7 and 8.4 GHz bands. The four consistent PPA values in both 4.7 and 8.4 GHz bands justify the higher RM value and the 180° added to the PPA in the 1.4 GHz band.
0943-242: Polarised flux seen at only one frequency in each of the lobes.
1138-262: *foll. lobe* - Has the highest RM for the whole sample. The linear fit to the data indicates that the high RM value is genuine. The values obtained from low and high resolution images are consistent with each other.
prec. lobe - Consists of multiple components which have large polarised flux but appear to be consistent with RM of zero, though the errors are large.
1324-262: *foll. lobe* - This is another high RM source with a good linear fit to the data.
prec. lobe - No polarised flux detected.
2025-218: *prec. lobe* - consists of multiple components, all of which are consistent with zero RM.
2036-254: *prec. lobe* - Another high RM source with an excellent linear fit. One of the frequencies in the 8.21 GHz is very noisy and polarisation is barely detected. However, the PPA appears to be consistent.
2104-242: *prec. lobe* - Two values of the RM appear to fit the data though the lower value provides a better fit.

4. Nature of the Faraday screen

The identity of the principal Faraday screen(s) responsible for the RM is discussed in this section.

4.1. Faraday screens non-local to the radio source

4.1.1. Galactic ISM

All the sources in the MRC/1 Jy sample, from which the HRRGs are drawn, were selected to lie at Galactic latitudes $|b| > 20°$ where the RM of the Galactic ISM is minimal. Further, the RM gradients in the ISM are known to be $\ll$10 rad m^{-2} over $\sim$1' arc (Simonetti & Cordes, 1986; Leahy 1987). The much larger gradients observed in the HRRGs (implied by the difference in the RMs of the two lobes which have a typical separation of $\lesssim 10''$ arc) indicates that the origin of the RM is extragalactic.

The RM contributed by the Galactic ISM was estimated by averaging the RMs of all known radio sources within a cone of 15°radius centred on the HRRG. The RM data and the method used are described in Simard-Normandin et al (1981) and Simard-Normandin & Kronberg (1980). The extreme RM values ($> 1.3\sigma$ from the mean) were discarded and the mean recalculated to obtain the values listed in Table 3. It was also confirmed that this mean value from the subsample was consistent with the median for the whole sample. However, when the RM values of the different sources within the cone were widely discrepant, the values listed in Table 3 are the mean values for the sources nearest to the HRRG; the 3 nearest sources (all with similar RMs) were considered for 1138-262 and the 4 nearest sources for 2025-218.

4.1.2. Intervening galaxies and clusters

Disk galaxies and the centres of rich clusters at low redshifts can introduce Faraday rotation in background radio sources. The probability of intersecting an object at redshift z along a line of sight is given by

$$dP = 1.9\,(\frac{R_c}{10\,kpc})^2\,(\frac{N_o(z)}{Mpc^{-3}})\,(\frac{1+z}{\sqrt{1+\Omega_o z}})\,dz, \qquad (3)$$

where R_c is the radius of cross-section and $N_o(z)$ is the comoving number density.[2]

Intervening clusters Kim et al. (1991) reported excess RMs in radio sources located behind the centres (inner 500 kpc) of Abell clusters which indicated that cluster cores introduce Faraday rotation in the background sources. From the observed density of $8.8.10^{-7}$ Mpc^{-3} of Abell clusters richer than Class 1 (Efstathiou et al. 1992) and assuming a constant co-moving space density between z = 0 and 1, the probability of intercepting the inner $500h^{-1}$ of a cluster along a line of sight is only $\sim$0.5%. This value is a robust upper limit since rather liberal values have been used for all the parameters. The small probability, coupled with the fact that not all clusters introduce large RMs makes it very unlikely that foreground clusters are the Faraday screens of the HRRGs.

Absorption-line Systems The abundance of disk galaxies and their presumed progenitors at high redshifts, the damped Lyα absorbers, can be estimated from their presence in the optical spectra of distant quasars. Their estimated line-of-sight number density, $n(z) = (0.015 \pm 0.004)\,(1+z)^{2.27\pm0.25}$ (Rao et al. 1995), gives a probability of $\sim$16% for intersecting one along a line of sight between z = 0 and 2.

It was believed that the presence of damped Ly$_\alpha$ systems (as against other absorption systems) in the optical spectra of quasars greatly increased the probability of *detection* of RM of extragalactic origin (ie. an RM larger than 3 $times$ the error after subtracting the galactic contribution) at radio wavelengths (Wolfe et al. 1992). However, the result was based on a heterogeneous sample of 5 quasars with damped Lyα absorbers. A more recent study of 11 radio quasars with damped Lyα absorbers (from a complete sample of 60 quasars) detected extragalactic RMs in only 2 sources (Oren & Wolfe, 1995). Eight of the 11 quasars had RMs less than 40 rad m^{-2} , all of which were smaller than the quoted errors.

Estimating the RM contribution of intervening objects in the spectra of compact quasars is very unsatisfactory because RMs can be estimated along only one line of sight per object. The single value makes it very difficult to separate the contributions from the Galactic ISM, intervening galaxies/clusters and regions local to the quasars (both nuclear and in the extended environment). On the other hand the RMs of extended radio sources provide diagnostics like the gradient in the values which have been used in this work to rule out the Galactic ISM.

An estimate of the RM contribution from the intervening systems may be obtained from RMs of 14 extended radio lobes in 7 galaxies at z $\sim$ 0.6–1.2 ($|b| > 20°$) (Pedelty et al., 1989). Seven of the 14 RM_{obs} values are < 10 rad m^{-2} and only 3 are greater than 40 rad m^{-2} (highest 60 rad m^{-2}). The variation of RMs across the lobes indicates that much of the RM is local to the radio galaxies.

[2] H_o = 50 km s^{-1} Mpc^{-1} and Ω_o = 1, unless otherwise mentioned, throughout this paper.

The small probability of intersecting disk galaxies and Lyα absorbers along the line of sight and the small RMs observed in many of them makes it very unlikely that they are responsible for the large RMs observed in HRRGs.

4.1.3. Gravitational lenses

It has also been suggested that many of the HRRGs may be lensed by intervening galaxies (Hammer & Le Fevre 1990). Lensed background radio sources may be preferentially selected in flux limited samples due to magnification of the intrinsic flux. If the lenses (at much lower redshifts) were the Faraday screens, the intrinsic RMs would be much smaller than estimated here and would also account for the large differences in the RMs of the two lobes. However, we find no preference for the brighter lobe to have a larger RM as would be expected in this model. Further the deep optical/IR images of these HRRGs show no other galaxies in the close vicinity except in the case of 0406-244 (see McCarthy et al. 1991a; Rush et al. 1996).

4.2. Faraday screens local to the radio source

Having argued that intervening systems are unlikely to be the Faraday screens of HRRGs in most cases, we shall ascribe all the RM to screens in the vicinity of the HRRGs themselves. The intrinsic RMs, corrected for cosmological redshifts, are listed in Table 3. In addition, the intrinsic RMs have also been calculated by subtracting the Galactic RM (GRM) from the observed RM before correcting for the redshift. We have listed the intrinsic RM values obtained by both subtracting and not subtracting the GRM because the uncertainties in many GRM values are an appreciable fraction of the values themselves.

It must be noted that significant RM contributions from damped Lyα systems at z $>$ 2 would change the identity of the Faraday screen (from local to the radio source to intervening galaxies) but would not alter the conclusion regarding RMs and magnetic fields at high redshift.

An examination of the highest RM measured in a source shows that four of the 13 sources have values in excess of 1000 rad m^{-2} with the highest value of 5911 rad m^{-2} in 1138-262 (z = 2.17). In fact, over half the sources have values of well over 500 rad m^{-2} (i.e. RM $> 500 + 3\sigma$ error) while only 3 sources are consistent with values $<$100 rad m^{-2} (RM - $3\sigma <$ 100). This is in sharp contrast to the much smaller fraction of high RM sources at z $<$ 0.5 (Taylor et al. 1992). It must be noted that higher resolution observations have always resulted in the detection of higher RM values in other radio galaxies; the RM values obtained from our low resolution observations may in fact be underestimating the highest RM in the HRRGs (see 0156-252 in this sample). These numbers are somewhat modified when the GRM corrected values of the intrinsic RM are used; however, the large RM sources, particularly those with values in excess of 1000 rad m^{-2} , are hardly affected by the GRM. The two other HRRGs with known RMs, 4C 41.17 at z = 3.8 and 0902+343 at z = 3.4, have intrinsic RMs of 6250 and 1100 rad m^{-2} , respectively (Carilli et al. 1994a; Carilli 1995).

Table 3. Intrinsic rotation measures in the lobes of MRC/1Jy galaxies at z > 2. The columns are redshift (z), remarks (R), observed RM (RM_{obs}), Galactic RM towards the source (GRM), intrinsic RM not corrected for Galactic RM (RM_{int} = RM_{obs} $(1+z)^2$) and intrinsic RM corrected for GRM (RM^G_{int} = (RM_{obs} - GRM)·$(1+z)^2$). The remarks are as described in Table 2.

source	z	R	RM_{obs} rad m^{-2}		GRM rad m^{-2}	RM_{int} rad m^{-2}		RM^G_{int} rad m^{-2}		
			Foll. lobe	Prec. lobe		Foll. lobe	Prec. lobe	Foll. lobe	Prec. lobe	
0015-229	2.01	l	8.3 ± 2.1	19.3 ± 1.9	7.9 ± 3.8	75 ± 19	174 ± 18	3 ± 39	102 ± 39	
0140-257	2.64	h	–	33.4 ± 63	4.4 ± 3.2	–	443 ± 837	–	385 ± 838	
0156-252	2.09	l	7.5 ± 1.7	–	8.2 ± 5.9	72 ± 16	–	-6 ± 59	–	
		a,l	82.0 ± 1.7	–		783 ± 16	–	705 ± 59	–	
		h	160 ± 31	–		1528 ± 296	–	1450 ± 301	–	
0316-257	3.13	l	0.6 ± 2.4	14.5 ± 2.4	7.2 ± 4.1	11 ± 40	247 ± 40	-112 ± 81	124 ± 81	
0349-211	2.31	l	54.8 ± 1.7	25.9 ± 2.2	18.1 ± 4.0	600 ± 19	284 ± 24	402 ± 48	86 ± 50	
0406-244	2.44	l,h	17.3 ± 2.6	74.4 ± 1.6	18.1 ± 4.0	205 ± 30	880 ± 19	-9 ± 56	666 ± 51	
		a,l,h	-59.6 ± 2.6			-705 ± 30		-919 ± 56		
1106-258	2.43	l,h	12.7 ± 1.9	38.7 ± 4.3	0.1 ± 31	150 ± 22	456 ± 50	150 ± 22	456 ± 50	†
1138-262	2.17	l,h	588 ± 22	31.1 ± 26	-26 ± 1.3	5911 ± 224	312 ± 258	6172 ± 224	573 ± 258	
1324-262	2.28	l,h	183 ± 20	–	-31 ± 3.5	1963 ± 216	–	2297 ± 219	–	
2025-218	2.63	h	-30.4 ± 77	42.5 ± 30	-22 ± 4.0	-400 ± 1020	560 ± 395	-110 ± 1021	850 ± 399	
2036-254	2.00	h	0.3 ± 25	-369 ± 48	-4.5 ± 13	2.7 ± 227	-3321 ± 429	2.7 ± 227	-3321 ± 429	†
2104-242	2.49	l	-10.0 ± 2.1	5.7 ± 7.0	0.4 ± 5.3	-122 ± 25	69 ± 85	-122 ± 25	69 ± 85	†
2139-292	2.55	l,h	-49.8 ± 2.0	10.3 ± 1.7	-2.2 ± 13	-628 ± 26	-129 ± 21	-628 ± 26	-129 ± 21	†

Note: The sources for which the intrinsic RMs have not been corrected for GRM are indicated by a † in the last column. In these sources, the uncertainty in the GRMs are much larger than the estimated values.

The RMs of the two radio lobes in each source show differences of several thousand rad m^{-2} .

Several sources in our sample show a rotation of more than 90° (Fig. 2); an internal screen, i.e. thermal plasma mixed with the synchrotron plasma, can be ruled out in such cases (Laing 1984). Going by the prevalence of external rotation in FR II radio sources, it is assumed here that the rotation occurs outside the emitting region in all the HRRGs of this sample; the rotation in the PPA of $< 90°$ seen in many of them is likely to be due to the small range in rest frame λ^2 at which they have been observed. One of the radio lobes in 0943-242 shows a higher fractional polarisation at a lower frequency, which may be due to an internal screen. However, higher resolution observations are required to confirm this as low resolution observations have the same effect as an internal Faraday screen in case of unresolved magnetic field structure.

All the high RM radio galaxies at low redshifts are known to be associated with dense environments; the radio sources are either compact (sub-galactic in size) or associated with cooling-flow clusters (Taylor et al. 1992, 1994). That the HRRGs, which are also presumed to be in dense environments, show large RMs is, perhaps, an indication that dense ambient gas plays a key role in forming a deep Faraday screen. Before going into the problem of Faraday screens at high redshift, we shall first outline briefly the situation in low redshift objects with high RMs.

Several workers have dealt with the problem of generating the large RMs seen in low redshift clusters. Using a typical intracluster medium (ICM) electron density of 0.01 cm^{-3}, the observed RMs of thousands of rad m^{-2} require magnetic fields of a few to tens of μG correlated over tens to hundreds of kpc (Perley & Taylor 1991; Taylor & Perley 1993; Taylor et al. 1994; Feretti et al. 1995). However, there is very little direct observational evidence of such strong magnetic fields on such a large scale. It is generally assumed that the fields are organised on the cluster core scales (100–200 kpc) and the magnetic fields are calculated by using these values of L in Eqn. 2. It has been suggested that the turbulence due to galaxies moving through the ICM generates the large scale magnetic fields (Jaffe 1980; Ruzmaikin et al. 1989). However, most non-linear calculations indicate that the magnetic fields generated cascade quickly to much smaller length scales and maintaining μG fields correlated over a kpc is a tough proposition; most models produce tenths of μG correlated over a few kpc at best (de Young 1992; Goldman & Rephaeli 1991). Indeed, there is observational evidence from the correlation analyses of RM variations in the transverse direction that the magnetic fields are tangled on scales of <1–5 kpc (Feretti et al. 1995; Perley et al. 1984; Ge & Owen 1993, Taylor & Perley 1993). The Laing-Garrington effect, wherein the radio lobe on the counter-jet side (presumably the farther lobe in the relativistic beaming models) is more depolarised, also indicates considerable tangling up of the fields in the ambient medium on scales much smaller than the radio lobes. It is difficult to envisage magnetic fields correlated over tens or hundreds of kpc along one direction while the correlation is only a few kpc in the perpendicular direction. However, it has been suggested that cluster cooling flows may result in such an anisotropy, though not to such a large degree (Soker & Sarazin 1990). Cooling material flowing into the deep potential well of clusters may result in the stretching (and alignment) of the frozen-in magnetic field in the radial direction. This may also result in a moderate ampli-

fication of the radial component. However, since the stretching of the field lines is due to differential infall as a function of radius, the radial alignment and amplification would be appreciable only in the case of cooling flows extending from several hundreds of kpc to an inner radius of 10–20 kpc.

Even if the field is stretched radially by a cooling flow, it must be noted that field reversals could occur on scales similar (apart from the stretching by a factor of few) to that seen in the transverse direction. This *random walk* situation should result in an RM distribution with zero mean and an rms given by $\sqrt{N}\cdot \mathrm{RM}_c$, where N is the number of individual cells along the line of sight and RM_c is the typical RM of an individual cell. So the distribution of RMs of a large number of independent pixels within a radio lobe obtained from sufficiently high resolution observations, should be a gaussian with a zero mean. However, high resolution observations of several sources have shown a gaussian RM distribution but with a non-zero mean of up to thousands of rad m^{-2} (for e.g. Taylor & Perley 1993), indicating that, the cooling-flow scenario, while likely, is not the whole answer. The non-zero mean RM may be a result of a Faraday screen in the immediate vicinity of the individual radio lobes.

As the previous discussion shows, it is not clear if the mechanisms proposed to generate and align large magnetic fields in low redshift galaxies are actually appropriate. Explaining the large RMs at high redshift is even more problematic due to the added constraint of insufficient time. The Universe was just a sixth of its present age at z = 2.5; it is not clear if the time available at those redshifts is sufficient for the mechanisms to generate and align strong magnetic fields on a large scale. We have investigated below several mechanisms to see if they are plausible at high redshifts.

4.2.1. High redshift cooling-flows

In the cooling-flow scenario, a mass M_t (total mass $\simeq$ baryonic (M_b) + dark matter (M_d); 10% in baryons) turns around from the Hubble flow at a redshift z_m and collapses by a redshift z_{coll} into an isothermal sphere with a temperature T_{vir} (due to virialisation). It is essential that the collapse occurs on a timescale (τ_{coll}) smaller than the cooling time-scale (τ_{cool}) so that much of the material is still outside the core. Further, the cooling timescale should be substantially smaller than the Hubble time (τ_H) at the redshift at which the galaxies are being observed. Subsequent cooling and the resulting slow and ordered infall of the material into the potential well is called a cooling flow. Cooling, being a function of density and hence radius, will lead to a radial gradient in the infall velocity. The timescale constraints define the inner and outer radii within which plasma cools and flows in. The differential infall within the cooling shell results in a radial stretching of the frozen-in magnetic field leading to correlated magnetic fields in that direction.

We consider below a simple model for the formation of a high redshift cluster with a cooling flow. The relationships governing the formation of a cluster, derived from rather general considerations of gravitational collapse, are given in Padmanabhan & Subramanian (1992) and have been reproduced below. The formation of a cooling flow is constrained by the requirements that (i) it is formed by z $\geq$ 2.5 (ii) $\tau_{coll} < \tau_{cool} < \tau_H$ as required by an ordered inflow and (iii) the central density of the cluster is not higher than what is observed in clusters/galaxies today, i.e. M $\lesssim 2.10^{11}\,\mathrm{M}_\odot$ in baryons within 10 kpc radius. The last constraint is not central to the cooling flow model but it ensures that the high redshift cluster in our model is consistent with the clusters seen at low redshifts.

$$\tau_H = (\frac{20}{3h})\,(1+z)^{-3/2} \tag{4}$$

$$z_m = 1.588(1+z_{coll}) - 1 \tag{5}$$

$$\tau_{coll} = [\tau_h(z_{coll})] - [\tau_h(z_m)] \tag{6}$$

$$V^2 = (1.56\ 10^4)\ M_t^{2/3}\ h^{2/3}\ (1+z_{coll}) \tag{7}$$

$$T_{vir} = (0.375)\ M_t^{2/3}\ h^{2/3}\ (1+z_{coll}) \tag{8}$$

$$\rho_t = (8.35\ 10^{-28})\,(\frac{V^2}{R^2+R_c^2}) \tag{9}$$

$$\tau_{cool} = \frac{0.008}{(N_b)\,(T^{-1/2} + 16\,f_m\,T^{-3/2})} \tag{10}$$

where, h is the Hubble's constant in units of 100 km s^{-1} Mpc^{-1}, V is the total velocity dispersion in the cluster in km s^{-1}, T is the temperature, ρ_t is the total density (dark + baryon) in gm cm^{-3}, N_b is the electron density in cm^{-3}, R is the radial co-ordinate of the isothermal sphere formed during the collapse and R_c its core radius. f_m takes metal enrichment into account for the cooling rate (f_m is 0.03 for primordial abundance and 1 for Solar abundance; See Peacock & Heavens 1990). The other symbols are as already described in the previous two paragraphs. All masses are in $10^{12}\,\mathrm{M}_\odot$, timescales in Gigayear, lengths in kpc and temperatures in 10^6 K.

We have used R_c = 10 kpc, f_m = 0.03 and h = 0.5 in the calculations which follow. We assume that 10% of the total matter is in baryons, the rest being dark matter. The dark matter component is not expected to deviate from its initial isothermal density profile even over 10 Gyr while the peripheral baryonic matter cools and accumulates at the centre of the cluster potential resulting in similar amount of dark and baryonic mass ($2.10^{11}\,\mathrm{M}_\odot$ each within 10 kpc) seen in galaxies at the centres of present day clusters. The constraint on the central density requires $[\mathrm{M_t}^{2/3}\,(1+\mathrm{z}_{coll})] \leq 68.5$. For $\mathrm{z}_{coll} \geq 5$, which is essential for forming cooling flows by z = 2.5, we get $\mathrm{M}_t \leq 4.10^{13}\,\mathrm{M}_\odot$. The virialised temperature would be $\sim 2{\cdot}10^7$ K. The cooling timescale depends on the baryon density and so will be a function of radius within this isothermal sphere. The upper and lower constraints on the cooling time (described previously) define the shell within the collapsed sphere where a cooling flow can operate. The numbers and the constraints used above limit the cooling-flow to between 20 and 35 kpc. The picture that emerges here for a cluster at z $\sim$ 2.5 is that of about 20 galaxies with a galactic scale cooling-flow.

The cooling-flows in low redshift clusters operate between $\sim$15 and 100–200 kpc. It is this ratio of 10 which is responsible

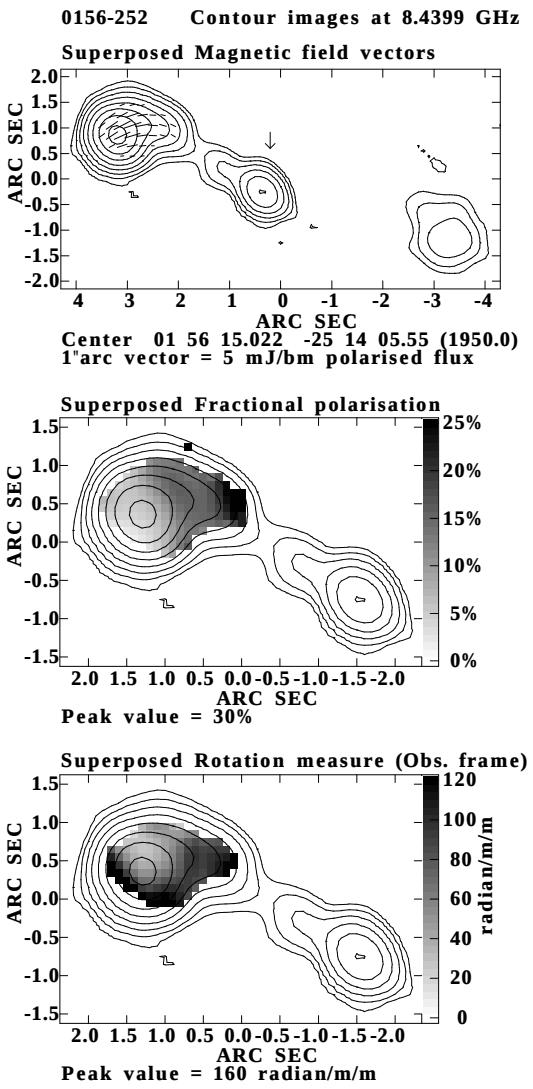

Fig. 3. Radio maps of 0156-252. The contour images at 8.44 GHz are superposed with (i) magnetic field vectors in the top image, (ii) grey scale of the fractional polarisation in the eastern lobe in the middle and the grey scale of the observed RM in the eastern lobe in the bottom image. The contour levels are 0.2 × -2, -1, 1, 2, 4, 8, 16, . . . mJy/bm. The beam size is $0\farcs65 \times 0\farcs5$ at 40° PA. The first contour level is $\sim 3 \times rms$ noise in the image. The polarisation images have been blanked below 5σ (0.3 mJy/bm at 8.44 GHz and 0.15 mJy/bm at 4.71 GHz).

for the alignment of the field. One can hardly expect any alignment of the magnetic field with the mini cooling-flows possible in HRRGs where the ratio is less than 2. Further, the 25 kpc size of the radio lobes hardly makes for any path length through a Faraday screen formed by such a cooling flow. Pushing the parameters to their limits would only change the cooling shell to between 30 and 45 kpc. The problem is even more severe to get cooling flows to form Faraday screens by z = 3.8! It seems unlikely that cooling flows play a significant role in generating Faraday screens at z > 2.

4.2.2. Large magnetised plasma clouds in the vicinity of the radio lobes

The large integrated RMs for the individual lobes and the differences between the two lobes suggests approximate sizes for the Faraday screens of a few kpc to ∼25 kpc (the lower limit from the presence of net RM and the upper limit from the difference). If the initial gravitational collapse is rapid and fragmentary (such a model is less constrained in parameter space and perhaps more likely than the cooling flow model), it would result in the formation of many clouds in the range of 10^8–10^{12} $M_\odot$ with little constraint on the total mass. These clouds could be responsible for the RMs seen in HRRGs. The optical continuum and line images of high redshift galaxies (see McCarthy 1993 and references therein) and the large differences in the properties of the two lobes of their radio sources (Pedelty et al. 1989; Athreya 1996) are indicative of the dense and clumpy environments at those redshifts required by this model.

A further refinement of this model is a collapsed object with correlated μG field in the path of the radio jet. A cloud of thermal plasma in the path of the jet would be stretched along the bow-shock. The resulting shear would stretch and align the magnetic field along a sheath around the radio hotspot. The passage of the shock would also increase the plasma density by a factor of 4 and may even amplify the magnetic field. A cloud with a baryonic density of just 1 particle cm^{-3} and 5 kpc diameter (baryonic mass of only 2.10^9 $M_\odot$) and a magnetic field of 1μG (all numbers refer to the unshocked cloud) can lead to an RM of several thousands of rad m^{-2} for a wide range of angles between the observer and the orientation of the bow-shock. An added appeal of this model is that the large differences in the RM values of the two lobes are naturally explained by Faraday screens local to each lobe rather than by a global screen. Structures in RM maps similar to what may be expected from a sheath around the bow shock have been seen in, for e.g., Cygnus A (Carilli et al. 1988), 3C 194 (Taylor et al. 1992a) and 0902+343 at z = 3.4 (Carilli 1995). Similarly, the RM structure seen in the high resolution images of 0156-252 in Fig. 3 is consistent with the above model; the highest RM values are in an arc in front of the hotspot and at a knot in the jet where it has bent considerably, presumably due to a collision with a clump of matter in the ambient medium.

5. Magnetic fields at z > 2

Regardless of the specifics of a Faraday screen model, the intrinsic RMs of several thousand rad m^{-2} require magnetic fields of the order of a μG correlated on scales of many kpc (see Eqn. 2) in the extended environments of galaxies at z > 2. The universe was just a sixth of its present age at z = 2.25 and only a tenth at z = 3.8. It is surprising that fields at such early times are similar to those found in galaxies and clusters today. These observations pose a considerable challenge to the models of magnetic field generation because of the small time available for amplifications at those redshifts.

The currently popular theory is that magnetic fields have arisen from amplification of a very weak seed field (10^{-21}–

10^{-19} gauss) by a dynamo mechanism (e.g. Zeldovich et al. 1983). Dynamos typically lead to an e-fold amplification over the dynamical time scale of the velocity field responsible for the dynamo action. The dynamo due to the turbulent motion of galaxies in the ICM would have dynamical timescales of the order of 10^8 yr or higher (galaxy sized 25 kpc eddies with speeds $\leq$ 1000 km s^{-1}). This would only lead to an amplification of 10^4–10^5, within the available 10^9 yr at z = 2.5, of the initial seed field of $\leq 10^{-19}$ gauss. This suggests that the Faraday screens cannot be more than $\sim$5 kpc (which reduces the dynamical timescale, providing sufficient time for the required number of cycles of amplification). However, this would necessitate larger magnetic fields to generate the same RM.

Lesch & Beck (1995) have suggested that the seed field amplification would proceed much faster in collapsed disk galaxies than in the ICM (see also Beck et al. 1994). The initial collapse would jump-start the process by amplifying the seed field by factors of about 10^4. Their calculations suggest that a dynamo in the rotating disk would further amplify the field by a factor of 10^{10} or higher by z $\gtrsim$ 2 if $z_{coll} \geq 5$. This correlated μG field is confined to the inner few kpc of the evolving disk galaxy. However, the amplification is a strong function of Ω and would be inadequate if Ω_o is much higher than 0.1. If this is indeed correct, it raises the possibility that the high RM radio sources are in the midst of (rich) clusters which already contain many collapsed systems and as such may be good candidates for targetted searches of high redshift clusters.

Another possibility is that the ambient thermal plasma is magnetised by the active radio source itself. The synchrotron plasma in the radio lobes have strong magnetic fields of hundreds of μG or even a magnitude higher in the active hotspot, particularly in powerful radio sources. The magnetic field is believed to be transported by the radio jet from the active nucleus. MHD instabilities (Bicknell et al. 1990) and turbulent diffusion may lead to the transport of the magnetic fields into the surrounding thermal plasma. However observations indicate that there is very little mixing of the thermal and the synchrotron plasma especially near the hotspot where the two are well separated by the bow-shock (Carilli et al. 1994b; Bohringer et al. 1993). It is believed that the radio jet evacuates the cluster medium along its path with very little mixing of the two media. A similar effect is seen in the galaxy 0902+343 (z = 3.4) with its line emitting gas anticorrelating with the radio structure (Carilli 1995). Even theoretically, it is not clear if the hotspot field can be diffused into the region around it on a timescale fast enough to produce a deep Faraday screen surrounding the hotspot before it moves ahead substantially (ie. within $\sim 10^6$ yr).

Tribble (1993) has suggested that synchrotron plasma from an extinct radio source may be responsible for magnetising the ICM. The absence of signs of a relic radio source in the vicinity of these HRRGs and the large times required for diffusion of the magnetic field to large distances, pushes the time of formation of the presumed earlier generation sources to even higher redshifts. The present understanding of what triggers a radio source is rather sketchy and whether the very short time available is sufficient for more than one radio source generation is not clear.

It has also been suggested that the galactic magnetic fields of today have arisen from a primordial magnetic field with a present day strength of 10^{-10} gauss and correlated over megaparsecs (Kulsrud & Anderson 1992). The field strength would go as $(1/S)^2$, where S is the cosmological scale factor. Such a primordial field would be of the order of 10^{-8} gauss at z_m = 9 (the redshift of turn around in section 4.2.1 - corresponding to z_{coll} = 5) and correlated over hundreds of kpc. Galactic and sub-galactic clumps condensing out of such material would have μG fields correlated over several kpc. However the nature of the processes which can generate such fields in the early universe is not clear.

6. Conclusions

- Multifrequency radio observations of 15 radio galaxies at z > 2 from the MRC/1Jy sample have resulted in the detection of large RMs. The Faraday screens responsible for the RM are most likely to be situated in the vicinity of the radio sources. Several sources have values in excess of 1000 rad m^{-2} with the highest RM of $\sim$6000 rad m^{-2} detected in 1138-262 (z = 2.17).
- The observations suggest that the extended medium around the sources is magnetised with μG fields correlated on scales of many kpc.
- Unlike at low redshifts, cluster cooling flows are unlikely to have a significant role in forming deep Faraday screens, since only galaxy-sized mini cooling flows (between $\sim$25 and $\sim$45 kpc) are possible at those redshifts, given the constraints of timescale and smooth infall.
- These observations pose a stiff challenge to the various mechanisms which have been proposed for generating magnetic fields, primarily due to the small time available for amplification of the initial seed field.
- We suggest that the the Faraday screens of these HRRGs are other collapsed galactic or subgalactic sized objects in the environs of the radio sources. Larger RMs may be produced if such objects are in the path of the radio jet; the collision and the subsequent shearing of such objects may result in the formation of deep Faraday screens capable of generating RMs of thousands of rad m^{-2} .
- If this scenario is indeed correct, the vicinity of the galaxies with large RMs at z > 2 may be good candidates for targetted searches for high redshift clusters.

Acknowledgements. RMA gratefully acknowledges the considerable amount of time spent by Dr. K. Subramanian in patiently explaining and discussing various aspects of magnetic field generation and galaxy formation. The work by WvB at IGPP/LLNL was performed under the auspices of the US Department of Energy under contract W–7405–ENG–48. We also thank the referee, Dr. P.P. Kronberg, for suggestions which have improved the manuscript. The VLA is operated by the Associated Universities Inc. under co-operative agreement with the National Science Foundation, USA.

References

Athreya, R.M. 1996, Multifrequency Studies of High Redshift Radio Galaxies, Ph.D Thesis, Univ. Bombay

Athreya, R.M., Kapahi, V.K., McCarthy, P.J., van Breugel, W. 1997a, MNRAS 289, 525

Athreya, R.M., Kapahi, V.K., McCarthy, P.J., van Breugel, W. 1997b, in preparation

Baars, J.W.M., Genzel, R., Pauliny-Toth, I.I.K., et al. 1977, A&A, 61, 99

Bicknell, G.V., Cameron, R.A., Gingold, R.A. 1990, ApJ, 357, 373

Bohringer, H., Voges, W., Fabian, A.C., et al. 1993, MNRAS, 264, 25p

Carilli C.L. 1995, A&A, 298, 77

Carilli, C.L., Owen, F.N., Harris, D.E. 1994a, AJ, 107, 480

Carilli, C.L., Perley, R.A., Harris, D.E. 1994b, MNRAS, 270, 173

De Young, D.S. 1992, ApJ, 386, 464

Efstathiou, G., Dalton, G.B., Sutherland, W.J., et al. 1992, MNRAS, 257, 125

Feretti, L., Dallacasa, D., Giovannini, G., et al. 1995, A&A, 302, 680

Ge, J.P., Owen, F.N. 1993, AJ, 105, 778

Goldman, I., Rephaeli, Y. 1991, ApJ, 380, 344

Hammer, F., Le Fevre, O. 1990, ApJ, 357, 38

Kapahi, V.K., Athreya, R.M., van Breugel, W., McCarthy, P.J., Subrahmanya, C.R. 1997a, In preparation

Kapahi, V.K., Athreya, R.M., Subrahmanya,, C. R., et al. 1997b, In preparation

Kim, K.-T., Tribble, P.C., Kronberg, P.P. 1991, ApJ, 379, 80

Kulsrud, R.M., Anderson, S.W. 1992, ApJ, 396, 606

Laing, R.A. 1984, In: Bridle, A.H., Eilek, J.A. (eds.) Physics of Energy Transport in Extragalactic Radio sources. Proc. NRAO Workshop # 9, Greenbank, p90.

Leahy, J.P. 1987, MNRAS, 226, 433

Leahy, J.P., Pooley, G.G., Riley, J.M. 1980, MNRAS, 222, 53

Lilly, S.J. 1989, ApJ, 340, 77

McCarthy, P.J. 1993, ARA&A, 31, 631

McCarthy, P.J., van Breugel, W., Kapahi, V.K., 1991a, ApJ, 371, 478

McCarthy, P.J., van Breugel, W., Kapahi, V.K., Subrahmanya, C.R. 1991b, AJ, 102, 522

McCarthy, P.J., Kapahi, V.K., van Breugel, W., et al. 1996, ApJS, 107, 19

McCarthy, P. J., van Breugel, W., Kapahi, V. K., et al. 1997, in preparation

Oren, A.L., Wolfe, A.M. 1995, ApJ, 445, 624

Padmanabhan, T., Subramanian, K. 1992, Bull. Astron. Soc. India, 20, 1

Peacock, J.A., Heavens, A.F. 1990, MNRAS, 243, 133

Pedelty, J.A., Rudnick, L., McCarthy, P.J., et al. 1989, AJ, 97, 647

Perley, R.A., Taylor, G.B. 1991, ApJ, 101, 1623

Perley, R.A., Bridle, A.H., Willis, A.G. 1984, ApJS, 54, 291

Rao, S.D., Turnshek, D.A., Briggs, F.H. 1995, ApJ, 449, 488

Rush, B., McCarthy, P.J., Athreya, R.M., Persson, S.E. 1996, Submitted to ApJ

Simard-Normandin, M., Kronberg, P.P. 1980, ApJ, 242, 74

Simard-Normandin, M., Kronberg, P.P., Button, S. 1981, ApJS, 45, 97

Simonetti, J.H., Cordes, J.M. 1986, ApJ, 310, 160

Soker, N., Sarazin, C.L. 1990, ApJ, 348, 73

Tabara, H., Inoue, M. 1980, A&AS, 39, 379

Taylor, G.B., Perley, R.A. 1993, ApJ, 416, 554

Taylor, G.B., Inoue, M., Tabara, H. 1992a, A&A, 264, 415

Taylor, G.B., Inoue, M., Tabara, H. 1992b, A&A, 264, 421

Taylor, G.B., Barton, E.J., Ge, J.P. 1994, AJ, 107, 1942

Tribble, P.C. 1993, In: Lynden-Dell, D. (ed.) Cosmical Magnetism. NATO Advanced Research Workshop, Institute of Astronomy, Cambridge, p140

Welter, G.L., Perry, J.J., Kronberg, P.P. 1984, ApJ, 270, 19

Wolfe, A.M., Lanzetta, K.M., Oren, A.L. 1992, ApJ, 388, 17

Ze'ldovich, Ya.B., Ruzmaikin, A.A., Sokoloff, D.D. 1983, Magnetic fields in Astrophysics. Gordon and Breach, London

This article was processed by the author using Springer-Verlag LaTeX A&A style file *L-AA* version 3.